Electrical and magnetic properties of FM/MgO/FM (FM = $Co_{90}Fe_{10}$, $Fe_{20}Ni_{80}$) heterostructures

Electrical and magnetic properties of FM/MgO/FM (FM $=$ Co$_{90}$Fe$_{10}$, Fe$_{20}$Ni$_{80}$) heterostructures

L Avilés-Félix [1,2]**, J González**[1,2]**, J E Gómez** [1,2] **and M Sirena**[1,2]

[1] Centro Atómico Bariloche, Instituto Balseiro—CNEA, Univ. Nac. de Cuyo, Av. Bustillo 9500, 8400 Bariloche, Rio Negro, Argentina
[2] Consejo Nacional de Investigaciones Científicas y Técnicas, Av. Rivadavia 1917 C1033AAJ CABA, Argentina

E-mail: lavilesf@gmail.com

CrossMark

Abstract

In this paper we present the development and characterization of FM/MgO/FM (FM $=$ Co$_{90}$Fe$_{10}$, Fe$_{20}$Ni$_{80}$) heterostructures. The magnetic order of the structures, magnetic anisotropy and interlayer exchange coupling were characterized by magnetization measurements. The influence of the substrate temperature during growth on the magnetic properties and topographical features of the bottom electrode was also explored. Higher values of the coercive field were achieved increasing the substrate temperature during deposition of the bottom electrode. Patterned magnetic tunnel junctions were grown on Si(1 0 0) and MgO(1 0 0). The junctions consist of square pillars with different areas (1600, 625, 100 and 25 μm^2) fabricated by optical lithography. $I(V)$ curves obtained with conducting atomic force microscopy of the patterned junctions were performed at room temperature in order to explore the reproducibility of the transport properties of the insulating barrier. The results show a more insulating behavior of the junctions grown on Si(1 0 0), with very good control and a high reproducibility of the transport properties of the MgO insulating barrier.

Keywords: magnetic tunnel junctions, microfabrication, interlayer exchange coupling, conductive atomic force microscopy

(Some figures may appear in colour only in the online journal)

1. Introduction

In recent years MgO-based tunnel junctions (MTJ) with metallic electrodes (Fe or CoFe) have been widely studied due to their potential high tunneling magnetoresistance (TMR) values. The high values of TMR make them ideal for the development of magnetic devices such as magnetic field sensors, spin torque oscillator devices [1], radio frequency amplification [2], etc. High values of TMR were predicted for these systems by Mathon *et al* [3] and Butler *et al* [4] in 2001. The origin of this effect is the coherent tunneling of electrons in epitaxial MTJ. First evidence of the tunneling through epitaxial MgO barriers was obtained by Yuasa *et al* [5] and Parkin *et al* [6] achieving significant MR ratios at room temperature.

Early experiments in MgO-based tunnel junctions involving amorphous MgO barriers have also shown promising results for technological applications showing high values of TMR at room temperature [7, 8] and it has been the foundations for the understanding of the coherent tunneling. Magnetic tunnel junctions used as reading heads of MRAM memories consists of several layers of thin films in order to artificially obtain a 'free' top electrode and a 'pinned' bottom electrode with different coercive fields. This structure assures two states of relative magnetization: parallel and antiparallel configurations.

One of the main difficulties for the fabrication of MTJ is to choose the appropriate electrodes in order to achieve the two different states of relative magnetization between the layers. It is also important to obtain a good reproducibility of the

transport properties of the insulating barrier, in order to assure a high reproducibility of the fabrication process. The two states of relative magnetization are usually influenced by the interlayer magnetic coupling between the layers of the magnetic tunnel junctions. Usually magnetostatic couplings are the more important types of interactions that could influence the coupling between the layers in multilayered structures. In this type of system, the dipolar or magnetostatic coupling strongly influence the switching behavior of the ferromagnetic electrodes and it is going to be discussed in the present work.

The optimization of the fabrication process of insulating barriers in MTJ is extremely important. The quality of the barrier helps to determine high number of parameters involved for the correct behavior of the junction [9, 10] (i.e. the attenuation length, the density of pinholes, the energy barrier, etc). Some effort to address this issue has been done in previous works [11, 12]. However, topographical and magnetic features of the electrodes also plays an important role on the electronic tunneling of the charge carriers through the barrier, therefore a good selection of the electrodes should also be made.

In this work we propose an alternative method for choosing two different materials as top and bottom electrodes in a MTJ, modifying the coercive field of one of the electrodes during its growth. $Co_{1-x}Fe_x$ alloys are commonly used both as part of the artificial antiferromagnetic layer in the pinned layer [13, 14] or as a ferromagnetic electrode of the junction [15] due to its high degree of spin polarization [6] ($\sim$85 %). $Co_{90}Fe_{10}$ was selected as top and bottom electrode of this work. $Fe_{20}Ni_{80}$ thin films were also used as top electrodes in order to study the interlayer magnetic coupling in magnetic junctions with different electrodes. Magnetic properties and topographical features of the electrodes will be discussed as well as the influence of the substrate on the transport properties of $Co_{90}Fe_{10}/MgO/Co_{90}Fe_{10}$ and $Co_{90}Fe_{10}/MgO/Fe_{20}Ni_{80}$ patterned magnetic tunnel junction.

The first part of the work involves the optimization and characterization of the CoFe electrodes. Topographical and magnetic measurements of single layers of CoFe were studied with atomic force microscopy (AFM) and vibrating sample magnetometry (VSM). Interlayer exchange coupling between $Co_{90}Fe_{10}$ (CoFe) and $Fe_{20}Ni_{80}$ (FeNi) layers will also be discussed. The second part of the work is focused in the fabrication of the patterned magnetic tunnel junctions and the use of conductive atomic force microscopy (CAFM) for the validation of the microfabrication process.

2. Experimental details

The different samples were grown on single crystal Si (1 0 0) and MgO (1 0 0) substrates by DC magnetron sputtering (CoFe and FeNi) and RF sputtering (MgO) from stoichiometric targets. Si and MgO substrates were cleaned for 15 min in acetone (5 min), isopropyl alcohol (5 min) and ultra-clean water (5 min) in an ultrasound cleaning machine. $Co_{90}Fe_{10}$ and $Fe_{19}Ni_{81}$ electrodes were grown using an argon pressure of 3 mTorr and 50W of DC magnetron sputtering. The MgO barriers were grown at room temperature using an Ar

pressure of 10 mTorr with a power of 30W for the radiofrequency sputtering. The crystalline structure of the ferromagnetic films were studied by standard $\theta - 2\theta$ x-ray diffraction. Topography and conductivity measurements were performed at room temperature on a Veeco Dimension 3100 scanning probe microscopy AFM with a CAFM module using a boron-doped diamond conductive tip with a spring constant between 20–80 N m^{-1}. The minimum detectable current in the CAFM is 50 pA and the maximum current limit is 480 nA, under a bias voltage ranging from 0.01 to 12V. All CAFM measurements were performed at room temperature and maintaining the same value of deflection setpoint (force exerted on the sample surface of 0.5V $\sim$ 5 μN). $I(V)$ curves were obtained with the CAFM in 'ramp' mode. This CAFM mode holds the conducting tip steadily on an untouched area of the sample's surface, then the applied voltage is ranged in the desired range while CAFM measures the current for the different values of the polarization voltage. The measurements have to be done in 'virgin' areas of the sample's surface (non-scanned areas) to reduce the chemical modifications due to the tip polarization voltage and to avoid damaging the barrier after several measurements. $I(V)$ curves were measured several times and on different areas in order to reduce the electrical noise and obtain representative data. The magnetic characterization was performed on a Lake Shore vibrating sample magnetometer model 73018 for hysteresis loops measured at room temperature. Micro-sized MTJ were obtained using optical lithography process in a UV mask aligner machine SUSS Microtec model MJB4 with a resolution printing down to 2 μm.

3. Results and discussion

3.1. Optimization of the top and bottom electrodes

In the first part of the work, the behavior of the coercive field (H_c) of 10 nm $Co_{90}Fe_{10}$ films as a function of the substrate temperature during the deposition was explored. Magnetization measurements of CoFe films grown on Si (1 0 0) at room temperature shows a saturation value of $\sim$1000 emu cm^{-3} and a coercive field of approximately 28 Oe. Angular variations for different orientations between the magnetic field and an arbitrary axis defined on the film indicates an uniaxial magnetic anisotropy behavior. Figure 1 shows the measured hysteresis loops along the easy and hard axis of a 10 nm CoFe film grown at room temperature on a silicon substrate. the remanence of the hysteresis loops as a function of the orientation between an arbitrary axis defined on the sample and the in-plane magnetic field is presented in the inset of figure 1 and is well fitted with a function of the form $A \sin^2 \alpha$ with a separation between maximum and minimum of 90° which confirms the presence of the uniaxial anisotropy.

As mentioned before, ferromagnetic electrodes in a MTJ should present different coercive fields. Therefore, the magnetic properties of 10 nm films as a function of the Si(1 0 0) substrate temperature during growth were studied. Samples were grown varying the substrate temperature from 250 °C to 550 °C. Figure 2 shows the $\theta - 2\theta$ x-ray diffraction profile for the films grown at different temperatures. The samples present
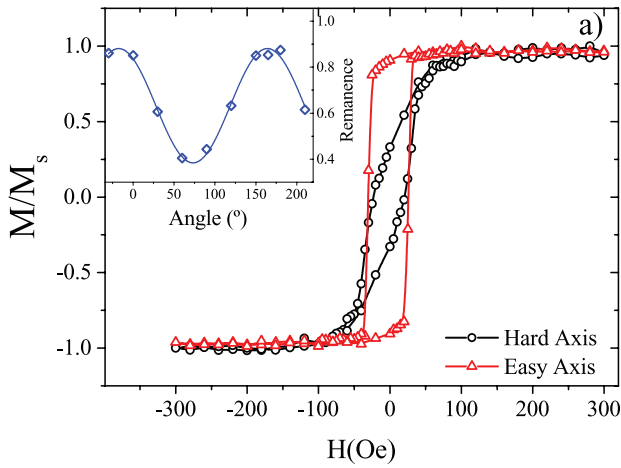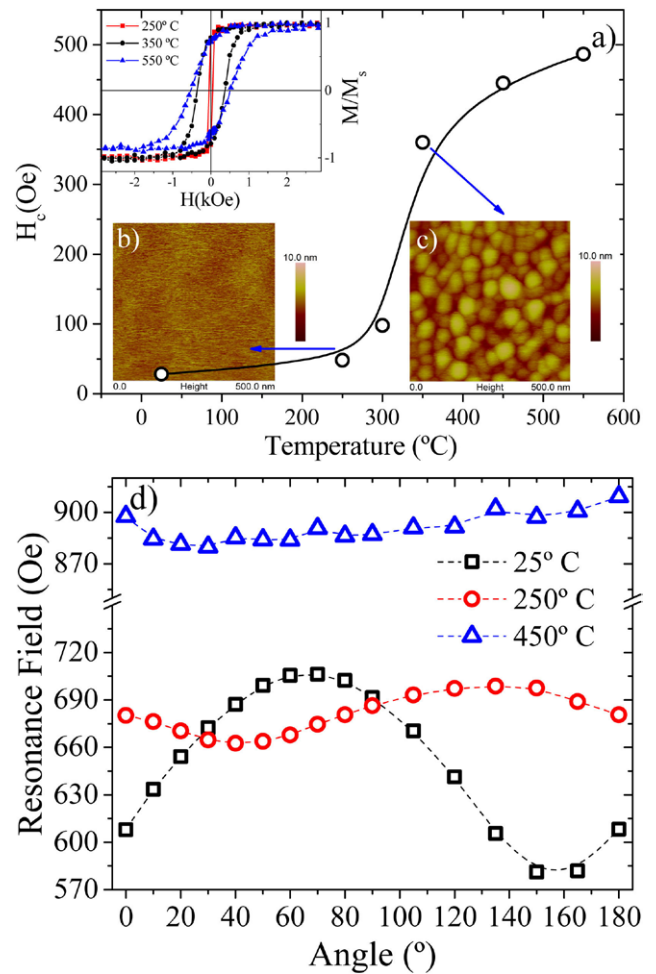
Figure 1. (a) Vibrating sample magnetometer measurements of 10 nm film of CoFe grown at room temperature. The magnetic field was oriented along the easy (△) and hard (○) anisotropy axis. Inset: behavior of the remanence as a function of the orientation between the in-plane magnetic field and an arbitrary axis defined parallel to the film's surface.
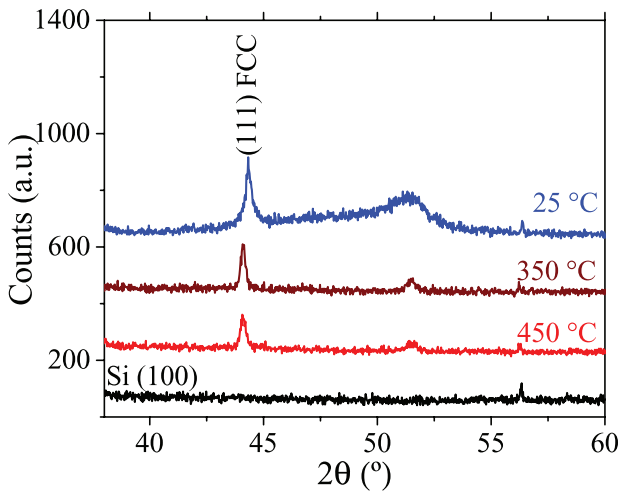
Figure 2. (a) $\theta - 2\theta$ x-ray diffraction profiles for the Si subtrate and CoFe films grown at different temperatures: 25, 350 and 450 °C.

Figure 3. (a) Coercive field of 10 nm films of CoFe as a function of the substrate temperature during the growth. The line is a guide for the eyes. Inset: normalized hysteresis loops of the films for different substrate temperatures. AFM topographic measurements at (b) 250 °C and (c) 350 °C. An increase in the grain size was observed with AFM for films grown at higher temperatures. (d) Ferromagnetic resonance measurements of CoFe films for different temperatures of the substrate during the deposition. The applied magnetic field was parallel to the plane of the films. Dotted lines are guides to the eyes.

a textured growth along the [1 1 1] FCC direction perpendicular to the substrate. Although, there is a high concentration of Co (hcp) in $Co_{90}Fe_{10}$, the presence of Fe atoms favors the FCC structure [16]. The [1 1 1] peak at 44.32°, corresponds to an interplanar distance of 3.53 Å.

Magnetic measurements revealed an increase of the coercive field (H_c) for temperatures above 250 °C (inset of figure 3(a)). The dependence of the H_c with the growth temperature presents an abrupt increment for temperatures between 250 °C and 350 °C, following by a linear increase for temperatures above 350 °C as shown in figure 3(a). The behavior of the coercive field could be directly related to the topographical features of the films as shown in figures 3(b) and (c). AFM measurements indicates an increase in the grain size of CoFe films grown at higher temperatures. Films grown at lower temperatures ($T < 300$ °C) present a small grain size. As the deposition temperatures increases, the grains became

bigger, with grain sizes between 20 and 40 nm of radius for deposition temperatures above 350 °C. The increase of the grain size in $Co_{90}Fe_{10}$ films grown at temperatures above 300 °C suggest a different growth mechanism of the single layers. As known, high deposition temperatures increases the mobility of the atoms at the substrate surface and in some cases favoring the formation of islands [17] during the first moments of the sputtering process.

A correlation of the coercive field with the grain size for polycrystalline films has been discussed in a previous work [18]. The origin of this dependence is described by the random anisotropy model [19]. This statistical model claims an increase of the coercive field H_c with the grain size D: $H_c \propto D^6$, which is valid as long as $D < l_{ex}$, where l_{ex} is the exchange length. In contrast with this model, the films grown in the present work show a smoother increase of the coercive field with the growth temperature, which indicate a non-linear dependence of the grain size with the growth temperature.

J. Phys. D: Appl. Phys. **49** (2016) 205303

L Avilés-Félix *et al*
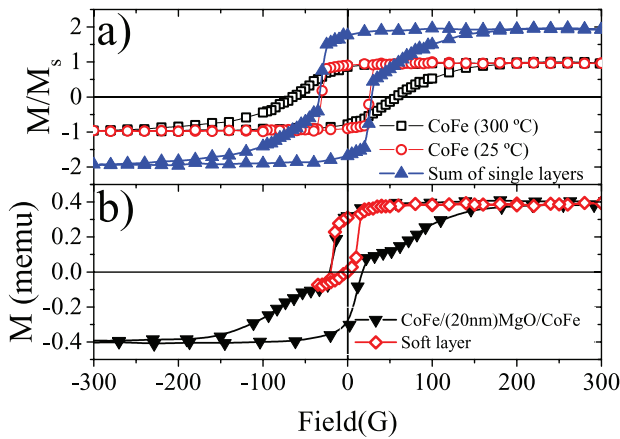
Figure 4. (a) Simulated hysteresis loop (▲) as a result of the sum of the two magnetization measurements of 10 nm CoFe films grown at 25 (○) and 300 °C (□). (b) $M(H)$ curve (▼) of a trilayer Si// CoFe(10 nm)(300°C)/MgO(20 nm)/CoFe(10 nm)(25°C) and minor loop (◊) corresponding to the magnetization of the top electrode.

Other groups achieved a similar behavior of the coercive field with the grain size in $Co_{50}Fe_{50}$ films varying the growth rate via the dc bias voltage during deposition [20].

For large $Co_{90}Fe_{10}$ grains compared with the exchange length l_{ex}, the direction of the magnetization is determined by the average of the effective anisotropies K_{eff} of each grain (magnetocrystalline, shape, induced, etc) and the formation of magnetic domains inside each grain. On the other hand, if the magnetic film is composed by small grains (uniform layer approximation), the magnetic moments tend to follow the preferential axis of magnetization determined by the competition between shape and magnetocrystalline anisotropy in the film. Exchange length l_{ex} is defined as [19] $l_{ex} = \sqrt{2A/4\pi M_s^2}$ (CGS units), where M_s is the saturation of the magnetic film and A is known as the *stiffness* constant, related to the difficulty of misalign parallel spins through the exchange integral. Large values of A means it is more difficult to misalign the spins, giving large exchange length values. Using the values $A = 3.14 \times 10^{-6}$ erg cm^{-1} [18] and $M_s = 1000$ emu cm^{-3} obtained from the magnetization measurements, the calculated value of l_{ex} is ~5 nm for our samples. The grain size of CoFe films grown at temperatures above 300 °C was higher than 40 nm, as shown by the topographic measurements. Therefore, the magnetization for these samples is the result of the average of the shape and magnetocrystalline anisotropy of the individual grains in the polycrystalline film, which induces the loss of a magnetization preferential axis.

In addition to an increase of the coercive field, the morphological change of CoFe films grown at higher temperatures modifies the magnetic anisotropy at room temperature. There is no change in the remanence of the hysteresis loops for different magnetic field direction obtained with the VSM for the samples grown at temperatures above 400 °C, which indicates the loss of the preferential axis of magnetization. This was also verified by ferromagnetic resonance (FMR) measurements with the external magnetic field applied parallel to the surface of the 10 nm films. As shown in figure 3(d) the

well-defined uniaxial anisotropy behavior observed for a CoFe film grown at room temperature diminishes for the films grown at higher temperatures disappearing for temperatures around 450 °C. FMR measurements also allows to obtain an approximation of the effective anisotropy H_{eff} (in magnetic field units) and its corresponding uniaxial anisotropy constant K_u in the plane of the film, according to the relation [21]:

$$H_r^{\perp} - H_r^{\parallel} \approx \frac{3}{2}H_{eff}, \qquad (1)$$

where $H_{eff} = 2K_u/M_s$ and $H_r^{\parallel}$ and $H_r^{\perp}$ correspond to the value of the resonance field (in Oe) measured with the applied magnetic field parallel and perpendicular with respect to the uniaxial anisotropy direction respectively. According to the equation (1), the effective field of the 10 nm CoFe Film grown at room temperature is $H_{eff} = 83$ Oe, corresponding to a uniaxial anisotropy constant $K_u \sim 3.25 \times 10^3$ erg cm^{-3}.

3.2. Interlayer magnetic coupling

In order to study the interlayer magnetic coupling in FM–MgO–FM systems, we fabricated by DC and RF sputtering trilayers using the same (CoFe–CoFe) and different electrodes (CoFe–FeNi) varying the MgO thicknesses. Bottom electrodes of the trilayer structure were grown at 300 °C. After the bottom electrode deposition, the single layers were cooled down to room temperature in an Argon atmosphere of 3 mTorr. Subsequently, the MgO barrier and the CoFe top electrode were grown at room temperature with the parameters previously described. The high temperature during the growth of the bottom electrodes (300 °C) assures a different coercive field (97 Oe) than the H_c of the top electrode (28 Oe).

Considering the magnetic properties of the single films, the hysteresis loop of the trilayer structure with 20 nm thickness of MgO could be predicted (assuming a completely decoupled system). The magnetization of the two CoFe layers independently follows the external magnetic field as a consequence of the thick insulating layer between them. The hysteresis loop of the trilayer system was simulated by summing the measured two normalized magnetization curves of the single layers (figure 4(a)).

In contrast, figure 4(b) shows the hysteresis loop of the Si(1 0 0)//CoFe(10 nm)/MgO(20 nm)/CoFe(10 nm) unpatterned trilayer structure measured with the VSM. Figure 4(b) also shows the minor loop of the soft layer. Although, both magnetic electrodes have the same thickness (10 nm), the magnetization jump corresponding to the top electrode is slightly larger than the corresponding to the bottom electrode, due to the reduction of the magnetization observed in the CoFe films grown at 300 °C, as shown in figure 3(d). The minor loop of the soft layer was slightly shifted to negative values of the magnetic field (≈ 3 Oe), indicating that the two layers are still coupled through the 20 nm MgO spacer. Angular dependence measurements (not shown) of the trilayer system reveal that the uniaxial anisotropy behavior remains for the soft layer. All $M(H)$ curves were measured along the easy axis.

Increased grain size of the bottom electrodes (CoFe films grown at 300 °C), increases roughness σ for both, the barrier

J. Phys. D: Appl. Phys. **49** (2016) 205303

L Avilés-Félix *et al*

and the upper electrode. As is known, high values of electrode-insulator interfaces roughness could lead to magnetically coupled systems due to an 'orange peel' coupling [22, 23], increasing the strength of the dipolar interaction between the layers separated by thinner spacers. The measured value of σ obtained from AFM measurements for single films, grown at temperatures above 300 °C, is $\sim$0.7 nm (2 unit cells of CoFe). The coupling energy of the system, J, is determined from the minor loop as the product between the shift of the $M(H)$ curve (minor loop) and the saturation of the soft layer, according to the equation [24]:

$$J = \Delta H M_s t, \qquad (2)$$

where M_s and t are the saturation and thickness of the soft layer respectively and ΔH is the shift of the $M(H)$ curve. Considering the previous equation and the value of the shift of the minor loop obtained experimentally, the calculated coupling energy is $J = 0.0028$ erg cm^{-2}. This energy obtained from the minor loop could be compared to the coupling energy due to the orange peel mechanism [25, 26]:

$$J^{Dip} = \frac{\pi^2}{\sqrt{2}} \frac{\sigma^2}{l} \mu_0 M_1 M_2 e^{\frac{-2\sqrt{2}\pi t_s}{l}}, \qquad (3)$$

where t_s is the spacer thickness, l is the period of the roughness σ, assuming a model of correlated roughness (wavelength model) [22] and M_1 and M_2 are the magnetization of the layers. Using equations (2) and (3), the calculated value for the period of the roughness was $l = 20$ nm. The magnitude of the periodicity correlates with the grain size of the bottom electrode grown at 300 °C.

Despite of the presence of two states of relative magnetization, that were observed for the CoFe/MgO/CoFe system, this effect is rapidly attenuated as we decreased the MgO thickness. In order to further study the interlayer magnetic coupling in our system, trilayers of MgO(1 0 0)//CoFe(10 nm)/MgO(x nm)/FeNi(10 nm) were grown varying the MgO spacer thickness ($x = 2$, 4 and 6 nm), with both electrodes grown at room temperature. Measured saturation values and coercive fields of $Fe_{20}Ni_{80}$ single thin films were $\sim$800 emu cm^{-3} and 2 Oe approximately.

Figure 5(a) shows the magnetization measurements along the easy axis of the MgO(1 0 0)//CoFe/MgO(x nm)/FeNi trilayers. In this figure, there is an abrupt jump of the magnetization corresponding to the coercive field of both ferromagnetic layers. The square shape of the magnetization curves, indicates the presence of a well defined uniaxial anisotropy of the films grown on MgO substrates. As it was expected, the coercive field H_c^{Py} of the Py layers is slightly larger for lower MgO thicknesses which indicates a weak interlayer coupling for a MgO spacer of $x = 2$ nm. It is well known that the interlayer exchange coupling influences the coercive fields of magnetic layers separated by an insulating barrier. The stronger the coupling, the coercive fields values would tend to a single coercive field value of the trilayer system.

On the other hand, coercive field values corresponding to the hard CoFe layers with 4 and 6 nm of the insulating barrier remains near the measured value for single films ($\sim$28 Oe).
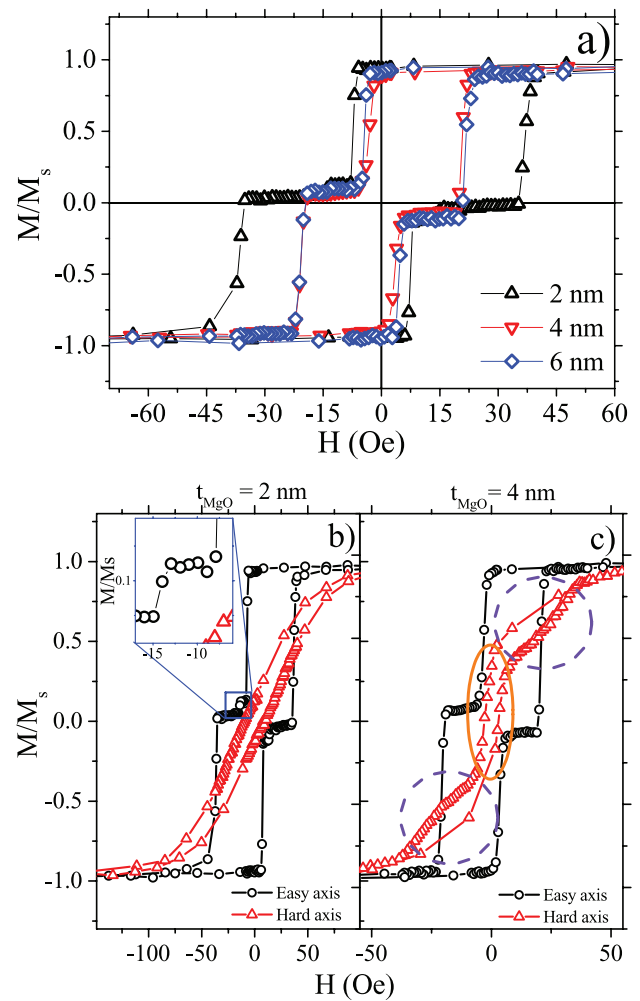
Figure 5. (a) Magnetization curves of the trilayer system MgO(1 0 0)//CoFe(10 nm)/MgO(x nm)/FeNi(10 nm) varying the MgO thickness. Inset: coercive field of the 10 nm FeNi film grown on Si(1 0 0) substrate with a MgO *buffer* of x nm. (b)–(c) $M(H)$ measurements of MgO//CoFe/MgO(x nm)/FeNi trilayer along the easy (○) and hard (△) axis with a MgO thickness of (b) 2 nm and (c) 4 nm. Inset of figure (b): zoom of the $M(H)$ curve near the second jump in the magnetization of the trilayer with 2 nm of the insulating barrier. (c) The hard axis of the FeNi and CoFe films are indicated with solid and dotted circles respectively (see text).

Interestingly, a higher value of H_c^{CoFe} was observed for a MgO spacer of 2 nm. This effect could be related to an unwanted variation of the growth parameters of the CoFe layer. In some cases the reproducibility of the coercive field values could be influenced by the growth parameters or even the used substrate. However, this increase of the coercive field is independent of the insulating thickness does not affect the coupling with the soft layer.

Hysteresis loop along the easy and hard axis of uniaxial anisotropy of the trilayers with MgO thickness of 2 nm and 4 nm are shown in figures 5(b) and (c) respectively. In figure 5(b) $M(H)$ curve for a MgO spacer of 2 nm along the hard axis is lineal indicating the presence of a single preferential axis of magnetization for the system. A zoom of the $M(H)$ curve along the easy axis (inset of figure 5(b)) reveals a second jump of the magnetization near 15 Oe. We attribute the second

jump observed in the $M(H)$ curve of the trilayer with MgO thickness of 2 nm, to the stepwise form of the CoFe/MgO and FeNi/MgO interfaces originated by the presence of pinholes in the barrier or regions where the thickness is lower than the expected. As known, most interfaces are rough and exhibit steps, which separate different terraces. The roughness of the insulating barrier as well as the presence of pinholes would directly affect the interlayer coupling through thinner MgO barriers (2 nm). The second jump was not observed for thicker spacers. In contrast, figure 5(c) shows the $M(H)$ loops for a MgO spacer of 4 nm. The form of $M(H)$ curve along the magnetization easy axis reveals that the two ferromagnetic layers of CoFe and Py are magnetically decoupled. The presence of an additional jump as in the 2 nm spacer was not observed in this sample. The form of the $M(H)$ curve along the hard axis for this sample, as superposition of the $M(H)$ curve along the hard axis of CoFe (dotted circle) and FeNi (solid circle) are clearly observed, and evidences the independent rotation of the magnetization of each magnetic layer. The results of the interlayer coupling between CoFe and FeNi layers grown on MgO substrates are promising for the development of magnetic devices.

3.3. CAFM electrical characterization

Complementary to the interlayer exchange coupling of the trilayer system we characterized the electrical properties of the MgO insulating barrier using conductive atomic force microscopy (CAFM). The typical characterization of the conductivity of the insulating barrier involves the study of the $I(V)$ response of the bilayer system (without an upper electrode). However, due to a non-reproducible physical contact between the tip and the barrier surface, an important variation of the $I(V)$ response is usually observed. To significantly reduce the fluctuation observed in the electrical characterization of the barrier, we measured the $I(V)$ response directly on the upper electrode of the trilayers after its delimitation by optical lithography as shown in the inset of figure 6.

Conducting atomic force microscopy measurements of the fabricated MTJ were performed in order to test the reproducibility of the electrical properties of the junctions. Inset of figure 6 shows an schematics of the CAFM measurements of $I(V)$ curves for the trilayer system. We characterized Substrate//CoFe/MgO(6 nm)/CoFe patterned tunnel junctions grown on two different substrates: MgO (1 0 0) and Si (1 0 0). $I(V)$ curves shown in figure 6 for the system grown on Silicon substrates present a very high degree of reproducibility. In order to compare the conductivity through magnetic junctions of different sizes, $I(V)$ curves were normalized with the junction's area to obtain the current density through the insulating barrier. Current density ($J(V)$) curves (figure 7) allow us to obtain a value of $J(1.5\ V) = 0.192 \pm 0.007$ nA μm^{-2}. The linear dependence of the current with the junction area (inset of figure 7) as well as the exponential increase of the current density as a function of the applied voltage are good indications that the tunneling seems to be the main mechanism for the electrical transport in these systems [27].
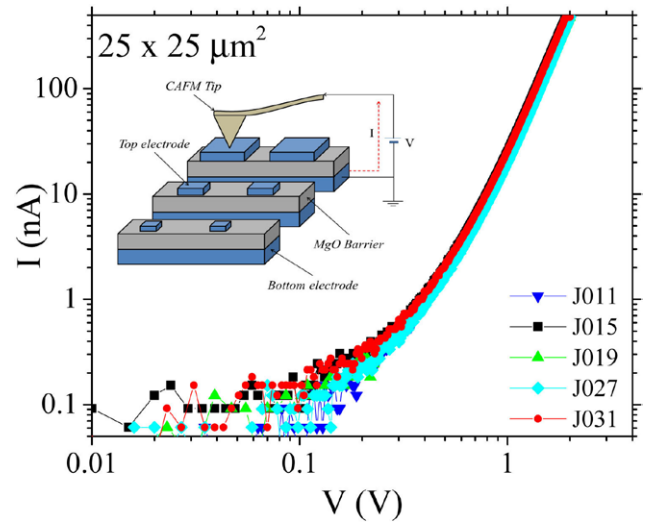

Figure 6. (a) $I(V)$ curves obtained with the CAFM for five different junctions of $25 \times 25\ \mu m$ in the system Si(1 0 0)//CoFe/MgO(6 nm)/CoFe. Inset: schematic of the CAFM measurements. The conductive tip was hold on the surface of the top electrode.
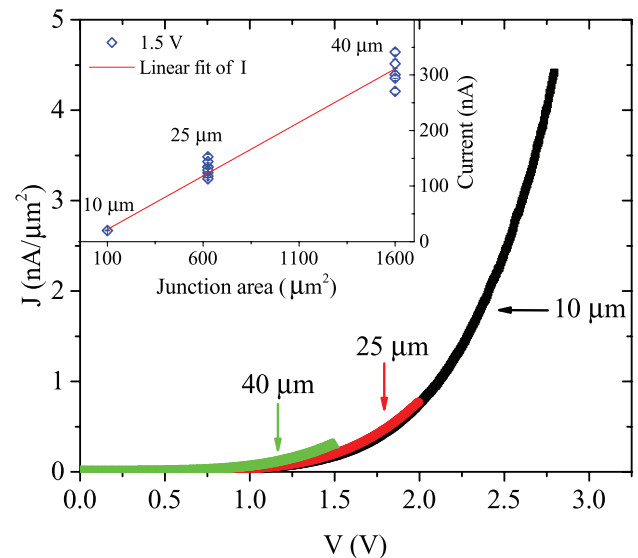
Figure 7. Current density $J(V)$ curves as a function of the applied voltage between the top and bottom electrodes of the system CoFe/MgO(6 nm)/CoFe grown on a Si substrate. Inset: tunneling current dependence as a function of the junction area for junctions of three different sizes: 10, 25 and 40 μm.

The same system, CoFe/MgO(6 nm)/CoFe, was grown on MgO(1 0 0) substrates. Figures 8(a)–(c) evidences a more insulating behavior for junctions grown on Si than in MgO substrates. Due to a lower value of effective roughness and a similar crystalline structure with the electrodes, MgO substrates would favor the crystallinity of the layers improving the conductivity through the insulating barrier. Previous studies on the influence of the substrate roughness on the transport properties of tunnel barriers have also shown an influence on the attenuation length and energy barrier for systems grown on different substrates [11, 28]. Calculated value of the current density for the trilayer system grown on MgO substrate was 1.29 nA μm^{-2} at 1.5 V, One order of magnitude higher

J. Phys. D: Appl. Phys. **49** (2016) 205303

L Avilés-Félix *et al*
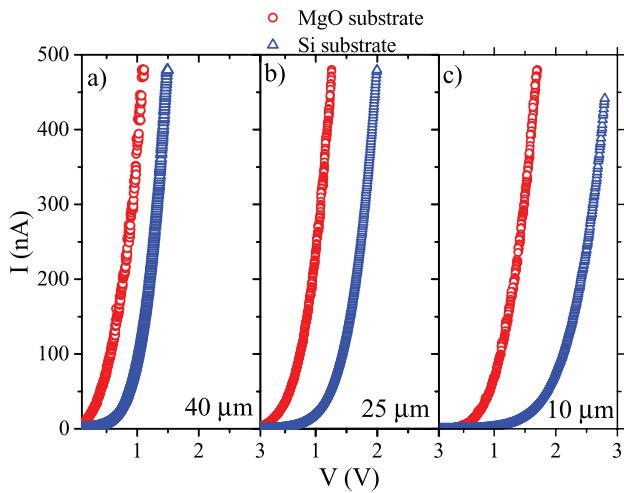
Figure 8. (a)–(c) *I*(*V*) curves of the system CoFe/MgO(6 nm)/CoFe grown on two different substrates: MgO (○) and Si (△). The sizes of the characterized junctions were (a) 40, (b) 25 and (c) 10 μm.

than the samples grown on Si(1 0 0). This is a strong indication of the substrate influence on the conductivity through the insulating barrier.

4. Conclusions

In the present work we have studied the magnetic and topographic properties of $Co_{90}Fe_{10}$ for its use as a bottom electrode in a FM–MgO–FM heterostructures. We observed an increase of the coercivity of 10 nm CoFe films increasing the substrate temperature during growth. A very good control in the coercive field of $Co_{90}Fe_{10}$ films was achieved. Substrate temperature during growth of the films influences the morphology and magnetic properties of single films of CoFe favoring grain formation and the loss of the magnetization preferential axis.

On the other hand, the interlayer magnetic coupling in FM–MgO–FM (FM = CoFe, FeNi) systems was discussed. Interlayer magnetic coupling between similar ferromagnetic layers was significantly influenced by the roughness of the interfaces due to the morphological features induced by the growth temperature of the bottom electrodes. The grain size of CoFe films grown at 300 °C was estimated using the dipolar coupling energy due to orange peel effects and it correlates with the values obtained by AFM measurements. We obtained ferromagnetic electrodes completely decoupled down to 2 nm of the insulating barrier for the samples grown on MgO substrates.

Micro-sized magnetic tunnel junctions of FM/MgO/FM (FM = CoFe and FeNi) grown on two different substrates were successfully fabricated presenting transport properties highly reproducible. We have used the CAFM as a tool for the electrical characterization, reproducibility and validation of the microfabrication process. A more insulating behavior was obtained for MTJ using Si(1 0 0) as a substrate and an increase of the current density (∼600%) was achieved for the system CoFe/MgO/CoFe grown on MgO(1 0 0) substrates. This indicates the importance of the substrate on the transport

properties of these systems. MgO (1 0 0) substrates are a better candidates for the fabrication of MTJ with MgO as an insulating spacer.

First results using four-probe electrical transport measurements of micro-sized (40×40 μm) magnetic tunnel junctions of CoFe/MgO(8 nm)/FeNi indicate a good quality of the insulating barrier. On the other hand *I*(*V*) response as a function of the temperature evidences a nonlinear dependence of the current with the voltage for different temperatures. The influence of the temperature on the differential conductance obtained allowed to determine the height of the energy barrier of CoFe–MgO–FeNi magnetic junctions (∼3 eV). A more detailed report of these results will be publish shortly.

References

[1] Kubota H *et al* 2013 *Appl. Phys. Express* **6** 103003
[2] Konishi K, Dixit D K, Tulapurkar A A, Miwa S, Nozaki T, Kubota H, Fukushima A, Yuasa S and Suzuki Y 2013 *Appl. Phys. Lett.* **102** 162409
[3] Mathon J and Umerski A 2001 *Phys. Rev.* B **63** 220403
[4] Butler W, Zhang X-G, Schulthess T and MacLaren J 2001 *Phys. Rev.* B **63** 054416
[5] Yuasa S, Nagahama T, Fukushima A, Suzuki Y and Ando K 2004 *Nat. Mater.* **3** 868
[6] Parkin S S P, Kaiser C, Panchula A, Rice P M, Hughes B, Samant M and Yang S-H 2004 *Nat. Mater.* **3** 862
[7] Yoshikawa M, Kitagawa E, Nagase T, Daibou T, Nagamine M, Nishiyama K, Kishi T and Yoda H 2008 *IEEE Trans. Magn.* **44** 2573
[8] Teixeira J M, Ventura J, Carpinteiro F, Araujo J P, Sousa J B, Wisniowski P and Freitas P P 2009 *J. Appl. Phys.* **106** 073707
[9] Bhutta K M, Schmalhorst J and Reiss G 2009 *J. Magn. Magn. Mater.* **321** 3384
[10] Evarts E R, Cao L, Ricketts D S, Rizzo N D, Bain J A and Majetich S A 2010 *IEEE Trans. Magn.* **46** 1741
[11] Avilés-Félix L *et al* 2012 *Nanotechnology* **23** 495715
[12] Sirena M, Avilés-Félix L, Carvacho Vera G A, Navarro Fernández H L, Steren L B, Bernard R, Briático J, Bergeal N, Lesueur J and Faini G 2012 *Appl. Phys. Lett.* **100** 012602
[13] Lee S, Han Y, Bae T, Hong J, Shim J, Kim E and Sunwoo K 2010 *J. Appl. Phys.* **108** 093902

J. Phys. D: Appl. Phys. 49 (2016) 205303

L Avilés-Félix et al

[14] Shu M-F, Canizo-Cabrera A, Hsu C-C, Chen C C, Wu J C, Li S C, Yang C-C and Wu T 2006 *J. Appl. Phys.* **99** 08R705

[15] Djayaprawira D D, Tsunekawa K, Nagai M, Maehara H, Yamagata S, Watanabe N, Yuasa S, Suzuki Y and Ando K 2005 *Appl. Phys. Lett.* **86** 092502

[16] Caruana Finkel A, Reeves-McLaren N and Morley N A 2014 *J. Magn. Magn. Mater.* **357** 87

[17] Michely T and Comsa G 1991 *Phys. Rev.* B **44** 8411

[18] Herzer G 1990 *IEEE Trans. Magn.* **26** 1397

[19] Coey J M D 2004 *Magnetism and Magnetic Materials* (Cambridge: Cambridge University Press)

[20] Vopsaroiu M, Georgieva M, Grundy P J, Vallejo Fernandez G, Manzoor S, Thwaites M J and O'Grady K 2005 *J. Appl. Phys.* **97** 10N303

[21] Yalcin O (ed) 2013 *Ferromagnetic Resonance—Theory and Applications* (Rijeka: Intech)

[22] Moritz J, Garcia F, Toussaint J C, Dieny B and Nozières J P 2004 *Europhys. Lett.* **65** 123

[23] Schrag B D, Anguelouch A, Ingvarsson S, Xiao G, Lu Y, Trouilloud P L, Gupta A, Wanner R A, Gallagher W J, Rice P M and Parkin S S P 2000 *Appl. Phys. Lett.* **77** 2373

[24] Faure-Vincent J, Tiusan C, Bellouard C, Popova E, Hehn M, Montaigne F and Schuhl A 2002 *Phys. Rev. Lett.* **89** 107206

[25] Wang D, Daughton J M, Qian Z, Nordman C, Tondra M and Pohm A 2003 *J. Appl. Phys.* **93** 8558

[26] Kools J C S, Kula W, Mauri D and Lin T 1999 *J. Appl. Phys.* **85** 4466

[27] Simmons John G 1963 *J. Appl. Phys.* **34** 1793

[28] Sirena M 2011 *J. Appl. Phys.* **110** 063923